Large area fabrication of high aspect ratio nano-cylinders on micro-pillars based on a colloidal crystal mask

Zexiang Yan, Ying Wang, Xingchang Zeng, Jiangbo Lu, Xianglian Lv, Weizheng Yuan, Yang He ✉

Key Laboratory of Micro/Nano Systems for Aerospace, Ministry of Education and Shaan'xi Key Provincial Laboratory of Micro and Nano Electromechanical Systems, Northwestern Polytechnical University, Xi'an 710072, People's Republic of China
✉ *E-mail: heyang@nwpu.edu.cn*

Published in Micro & Nano Letters; Received on 19th June 2020; Revised on 27th October 2020; Accepted on 8th November 2020

The combination of microstructures and nanostructures has broad application prospects. However, most existing methods are oriented to fabricating microstructures and nanostructures separately, and the fabrication of nanostructures on a microstructured surface at the wafer level is rarely studied. In this work, a new method of fabricating large-area high aspect ratio nano-cylinders on micro-pillars based on a colloidal crystal mask is proposed. An experimental device for stripping and draining was designed to create a polystyrene colloidal crystal mask. Together with reactive-ion etching and metal-assisted chemical etching, high aspect ratio nano-cylinders on micro-pillars with controllable size were obtained on a 4-inch silicon wafer. Wetting tests were performed on four groups of fabricated structures of different sizes, and the results showed that all samples were superhydrophobic. Thus, a method for fabricating uniform, size-controllable, large-area high aspect ratio nano-cylinders on micro-pillars with great potential as a superhydrophobic engineering material is proposed.

1. Introduction: Nanostructures on a microstructured surface (hereafter referred to simply as a micro–nanostructure) are gaining increased attention for their potential applications in the fields of anti-icing [1, 2], superhydrophobic materials [3], drag reduction [4], oil–water separation [5], biochemical sensors [6], bionics [7], medical science [8], optics [9] and so on.

In recent years, a great number of methods for manufacturing large-area microstructures and nanostructures such as micro-imprinting [10], nanosecond laser texturing [11, 12], hot embossing [13], nanoimprint lithography [14, 15], and nanosphere photolithography [16] have been proposed. However, many studies have proven that micro–nanostructures have higher stability and better performance than simple microstructures or nanostructures [17, 18]. Several attempts have been made to fabricate micro–nanostructures through various techniques, including self-assembly [19], nano-casting [20], chemical etching [21], electrochemical machining [22], and deep reactive-ion etching (RIE) [23]. Limited research has been conducted on micro–nanostructures for large-area manufacturing. Wu *et al.* [24] obtained nanostructure-covered conical microstructures on plastic parts through injection moulding with a large-area pattern (3×3.8 cm^2). The fabrication of large-area micro–nanostructures needs to fulfil the requirements of practical applications. For example, their anti-fouling property can increase the efficiency of solar cells by preventing the deposition of liquid and solid contaminants. Thus, developing a simple and controllable method of preparing large-area micro–nanostructures is potentially of wide applicability.

As shown in Fig. 1, a method of fabricating large-area high aspect ratio nano-cylinders by combining the method for the preparation of a large-area monolayer colloidal crystal mask [25] with metal-assisted chemical etching [26] is proposed. First, a polystyrene (PS) nanosphere suspension was spin-coated onto a silicon wafer treated with oxygen plasma. Microstructures were prepared by lithography and inductively coupled plasma (ICP) etching technology before treatment with oxygen plasma. Second, the spin-coated wafer was stripped to obtain high-quality monolayer PS colloidal crystals on the liquid surface, and then these crystals were deposited onto the microstructures through draining. Third, the diameter of the PS nanospheres was adjusted by RIE. Fourth, deposition of an Ag film and the nanostructure through Ag-assisted etching was achieved. After removing the Ag film and PS nanospheres, a 4-inch wafer of high aspect ratio nano-cylinders on micro-pillars was finally obtained. The liquid contact angle (CA) of the micro–nanostructures was measured to analyse their wettability.

2. Experiments

2.1. Preparation of PS colloidal crystal and microstructure: A PS nanosphere suspension with an average particle diameter of 909 nm (SD = 27 nm; 5% w/v; Microparticles GmbH, Germany) was selected. To reduce the free energy of the colloidal crystal solution, the 5% (w/v) PS suspension was centrifuged and diluted with ethanol (70%, Guangzhou Suno Chemical Co., Ltd) and deionised water to 2.5% (w/v). Then, 0.01% (w/v) surfactant Triton X-100 (Beijing Solarbio Technology Co., Ltd) was added and mixed evenly (the surfactant volume was one-third of the volume of PS suspension). A silicon wafer was placed in a plasma cleaner (YZD 08-5C, Beijing Huiguang Venture Technology Co., Ltd), and oxygen plasma treatment was performed for 5 s to make it hydrophilic. A total of 250 µl of 2.5% (w/v) PS nanosphere suspension was dropped onto the silicon wafer centre, and the mixture was allowed to stand for 1 min. The silicon wafer was placed on a spin coater (SC100-SE, Best Tools LLC, USA) and spun at 800 rpm for 75 s. A 4-inch colloidal crystal was obtained.

The micro-pillars were firstly fabricated as the substrate of the nano-cylinders. By lithography technology, the designed micro-pillar structure was transferred onto the silicon wafer, and then the silicon micro-pillar structure was formed by ICP etching.

2.2. Deposition of PS colloidal crystal mask on micro-pillars by stripping and draining: The deposition of the PS colloidal crystal was the key process to realise the controllable fabrication of the nano-cylinders on micro-pillars. An experimental device allowing stable and controllable stripping and draining was designed to ensure that the PS colloidal crystal was monolayered and close-packed. The experimental device (Fig. 2) was composed of a micro-stepping motor, a screw, a sliding platform, a holder, a polytetrafluoroethylene (PTFE) layer, a conical container, and a polyvinyl chloride (PVC) water pipe. The upper and lower diameters of the conical container were 200 and 150 mm, and the height was 125 mm. The motor-driven screw drove the silicon

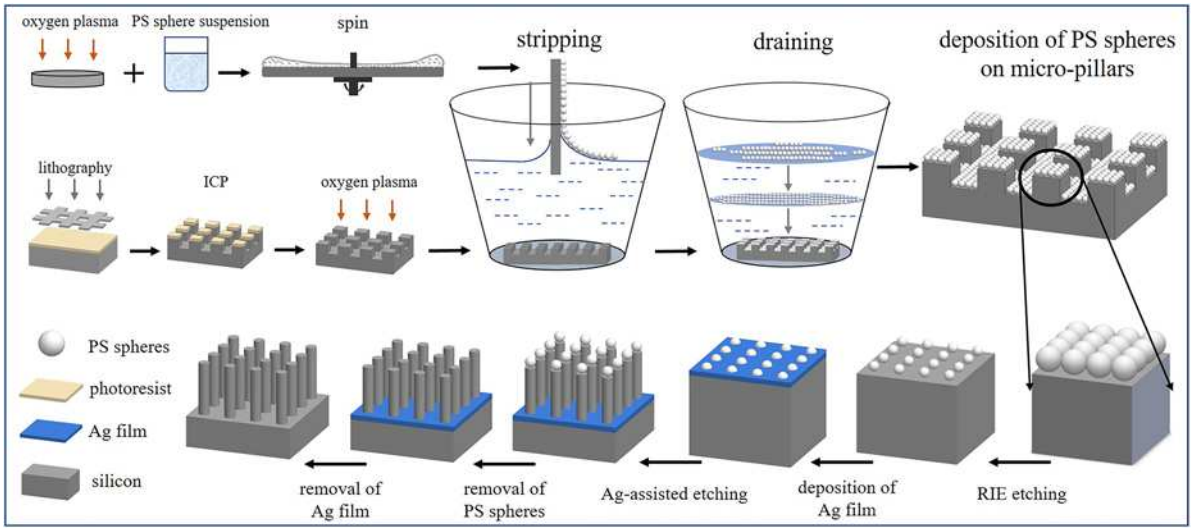

Fig. 1 *Fabrication of large-area, high aspect ratio nano-cylinders on micro-pillars*

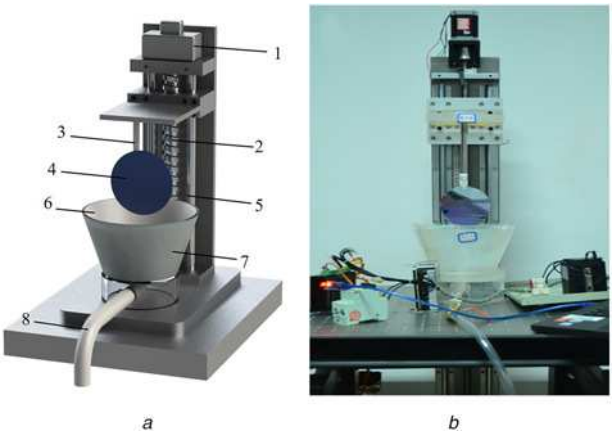

Fig. 2 *Experimental device for stripping and draining*
a 3D design schematic: 1, micro stepping motor; 2, sliding platform; 3, holder; 4, silicon wafer; 5, screw; 6, PTFE layer; 7, conical container; 8, PVC water pipe
b Actual apparatus

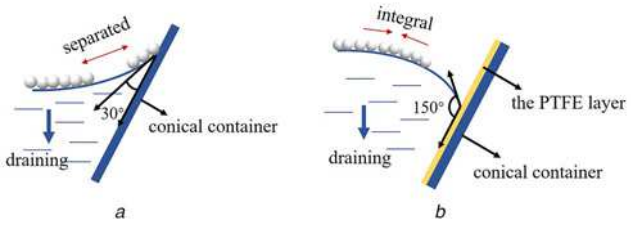

Fig. 3 *PTFE layer for maintaining the integrity of the PS colloidal crystal mask*
a Without a PTFE layer
b With a PTFE layer

wafer up and down, and the PS colloidal crystal on the silicon wafer was stripped onto the liquid surface. The experimental parameters were as follows: ambient temperature 20°C; solvent volume 2.5 l (ethanol:water = 1:2); and the wafer was pulled down at a rate of 1 mm/s. Thus, a monolayer PS colloidal crystal mask floating on the liquid surface was obtained.

After the stripping was completed, the silicon master was pulled out at a speed of 3 mm/s. When the silicon wafer was about to be lifted onto the liquid surface, 20 µl of 0.5% (w/v) Triton X-100 surfactant was added dropwise onto the liquid surface. Consequently, the PS colloidal crystal mask was gently pushed away and the Si wafer was subsequently pulled out without the PS colloidal crystal reattaching.

When the liquid level was stabilised, the flow rate of the drain valve was adjusted to control the draining speed until the colloidal crystal mask was deposited onto the microstructure at the bottom of the conical container. The conical container was made of plexiglass with a liquid CA of about 30° as shown in Fig. 3*a*. The liquid surface was in a stretched state during the draining process, which led to the PS colloidal crystal mask being separated. Since PTFE is hydrophobic with a liquid CA of about 150°, a layer of PTFE with a thickness of 4 mm was attached to the inner wall of the conical container to maintain the mask's surface integrity, as shown in Fig. 3*b*.

The drop rate of the liquid surface was selected to be 1 mm/s to minimise the defects. Finally, by evaporation at room temperature, a large-area, monolayer, close-packed PS colloidal crystal mask was formed on the microstructure surface.

2.3. Fabrication of high aspect ratio nano-cylinders on micro-pillars: RIE (radio frequency power, 50 W; pressure, 100 mTorr; SENTECH Etchlab 200) was used to adjust the diameter of the PS nanospheres. Ag film was deposited onto the surface of the structures obtained, with thicknesses ranging from 100 to 200 nm, using a 1.4×10^{-4} Pa vacuum, and an evaporation source temperature of 1050°C. Using the PS nanospheres as a mask, the silicon substrate was etched with Ag assistance, and nano-cylinder arrays were fabricated on top of the micro-pillars. Hydrofluoric acid (4.5 mol/l) and hydrogen peroxide solution (0.45 mol/l) were mixed to prepare the Ag-assisted etching solution. By controlling the etching time, nano-cylinder arrays with different heights were prepared. After removing the PS colloidal crystal mask and the Ag film, the large-area high aspect ratio nano-cylinders on micro-pillars were obtained.

2.4. Wetting-performance tests: Static contact-angle tests were performed on different sizes of micro-pillars and nano-cylinders on micro-pillars, and their wettability was compared and analysed. The CAs of surfaces were measured with an optical goniometer (OCA15EC, Data Physics Company Ltd., Germany). For all measurements, 5 µl of deionised water droplets were used. Each value was measured thrice in different areas and then averaged to

doi: 10.1049/mnl.2020.0345

ensure accuracy. In the experiment, the ambient temperature was set as 20 ± 1°C, and the relative humidity was maintained at 30 ± 2%.

3. Results and discussion

3.1. Surface morphology: The large-area high aspect ratio nano-cylinders on micro-pillars were observed by a SEM (VEGA3 SBH, TESCAN Company Ltd), and the results are shown in Fig. 4. With PS nanospheres of 909 nm average diameter, this method can fabricate arrays of nano-cylinders with diameters of 200–900 nm and heights of 300–900 nm.

3.2. Drop rate of the liquid surface: In the draining process, the most influential factor was the liquid surface drop rate v. The liquid flow rate Q was kept as a constant during experiments, controlled by a flow control valve, and was calculated as follows:

$$Q = Sv = S_b v_b = \left(\frac{150}{2}\right)^2 \pi v_b \ (\mathrm{mm}^3/\mathrm{s}) \tag{1}$$

where S is the liquid surface area, S_b is the bottom area of the conical container (the diameter of which is 150 mm), v is the liquid surface drop rate, and v_b is the liquid surface drop rate at the moment where the PS colloidal crystal mask was about to deposit on the micro-pillars. The liquid surface area was approximated as the bottom area of the conical container since the PS nanospheres were about to deposit on the bottom of the container. Drop rates of the liquid surface $v_{b1} = 0.5$ mm/s, $v_{b2} = 1$ mm/s, $v_{b3} = 2$ mm/s, and $v_{b4} = 5$ mm/s were set to observe the quality

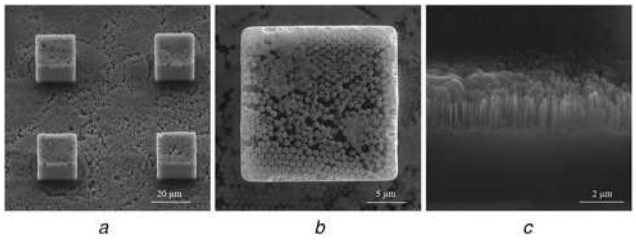

Fig. 4 *Surface morphology*
a High aspect ratio nano-cylinders on micro-pillars
b Top view of nano-cylinders on micro-pillars
c Side view of nano-cylinders on micro-pillars

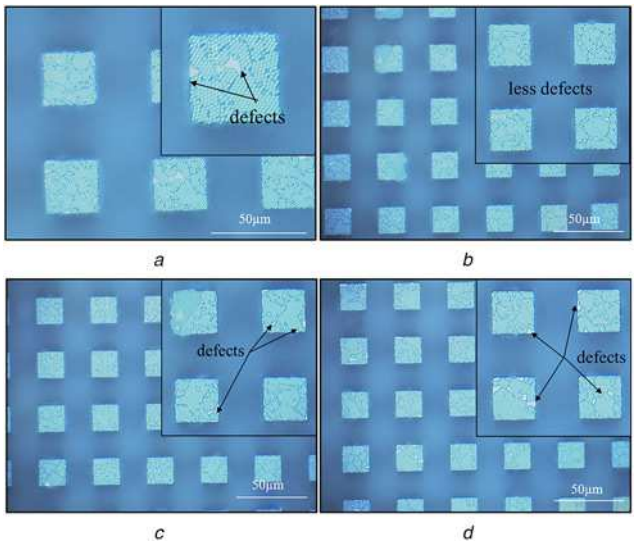

Fig. 5 *Effect of the drop rate on the quality of PS colloidal crystal mask*
a Drop rate $v_{b1} = 0.5$ mm/s
b Drop rate $v_{b2} = 1$ mm/s
c Drop rate $v_{b3} = 2$ mm/s
d Drop rate $v_{b4} = 5$ mm/s

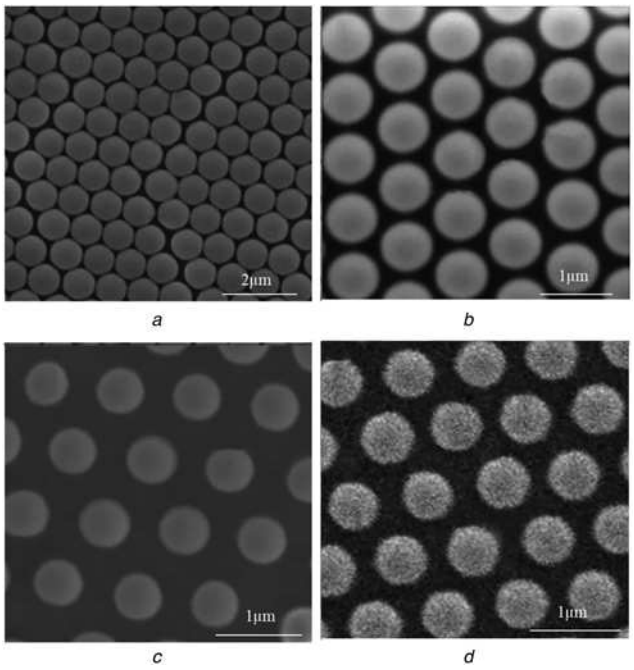

Fig. 6 *SEM images of PS nanospheres after different etching times*
a Etching for 60 s
b Etching for 90 s
c Etching for 120 s
d Etching for 130 s

Table 1 Diameter of PS nanospheres after different etching times

Etching time, s	0	60	90	120	130	150
diameter 1, nm	923	823	707	565	458	304
diameter 2, nm	912	838	708	558	446	297
diameter 3, nm	906	834	711	568	453	280
average diameter, nm	914	832	709	564	452	294

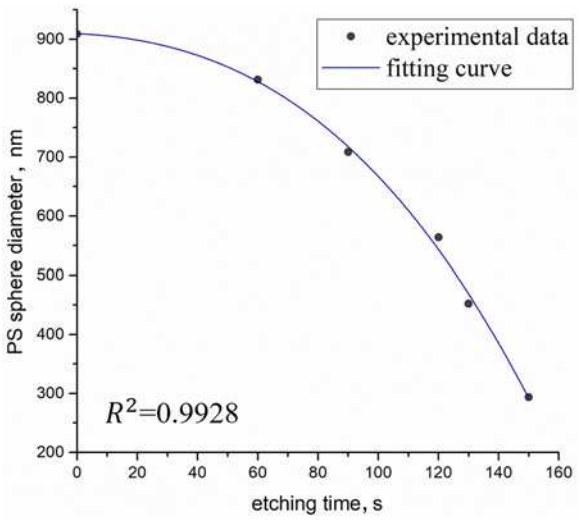

Fig. 7 *Graph of the diameter of PS nanospheres with etching time*

of the PS colloidal crystal mask on micro-pillars. Fig. 5 shows the effect of the drop rate on the quality of the PS colloidal crystal mask. In the draining process, the distance between PS nanospheres was reduced due to the shrinkage of the liquid surface. When the drop rate was appropriate, the PS colloidal crystal mask was uniform and dense, as shown in Fig. 5*b*. If the drop rate was too low, attraction between the PS nanospheres caused by the surface shrinkage was not strong enough to make the PS nanospheres uniformly close to each other, therefore voids would show as in Fig. 5*a*. If the liquid surface dropped too fast, the defects in the PS colloidal crystal film increased due to liquid fluctuation as shown in Figs. 5*c*, and *d*. Results of repeated experiments and comparisons revealed that when the drop rate was $v_{b2} = 1$ mm/s, the PS colloidal crystal deposited onto the micro-pillars had the fewest defects.

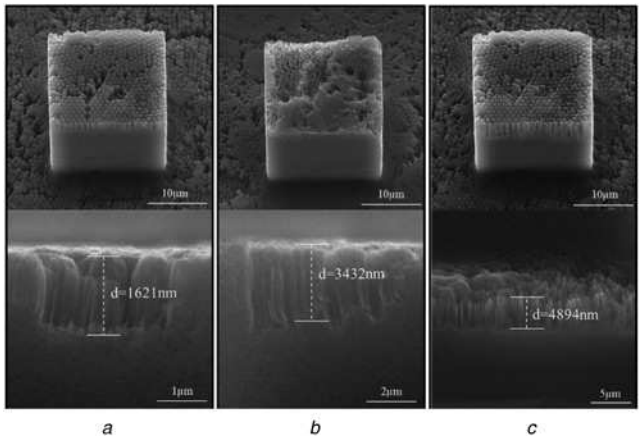

Fig. 8 *SEM images of nano-cylinders under different etching times*
a Etching for 4 min
b Etching for 8 min
c Etching for 12 min

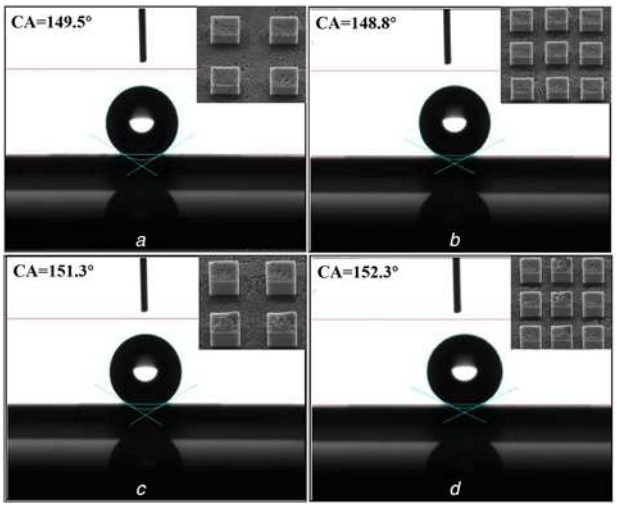

Fig. 9 *Static contact-angle results of micro–nanostructures (samples 1–4)*
a $h1 = 20$ μm, $b = 20$ μm
b $h1 = 20$ μm, $b = 10$ μm
c $h1 = 40$ μm, $b = 20$ μm
d $h1 = 40$ μm, $b = 10$ μm

3.3. Adjustment of the diameter of PS nanospheres: The diameter of the nano-cylinders was determined by the diameter of the PS colloidal crystal nanospheres. The RIE time was the key parameter determining the diameter of the PS nanospheres. The effect of different etching times on the diameter of the nanospheres was studied. Figs. 6*a–d* show SEM photographs of PS nanospheres after different etching times. The diameters of the PS nanospheres after 60, 90, 120, 130, and 150 s etching are shown in Table 1.

Using a cubic polynomial curve-fitting method, the relationship of the diameter of PS nanospheres with etching time is shown in Fig. 7, with $R^2 = 0.9928$. The diameter of the PS nanospheres decreased faster with a prolonged etching time. PS nanospheres with different diameters can be obtained by controlling the etching time.

3.4. Adjustment of nano-cylinder height: As the reaction time progressed, the silicon substrate with Ag film reacted with the etching solution, whereas the silicon substrate covered by the PS colloidal crystal mask remained unchanged. Consequently, nano-cylinders with preset heights can be obtained by controlling the time.

Reaction times of 4, 8, and 12 min were selected for experiments. Fig. 8 shows SEM images of nano-cylinders after different etching times. By controlling the reaction time, nano-cylinders on micro-pillars with different heights were obtained.

3.5. Wetting-performance test result: The CA is usually used to characterise the surface wettability, which is affected by the morphology and geometric dimensions of a structure. The wettability of four different sizes of high aspect ratio nano-cylinders on micro-pillars was tested, and results are shown in Fig. 9. Four samples with different sizes of micro-pillars without a nanostructure on top were set up as experimental control groups. The static CA results for both structures are listed in Table 2. Fig. 10 shows the definitions of the quantities tabulated.

Table 2 shows that the static CAs of the four nano-cylinders on micro-pillars were all between 150° and 155°, showing a superhydrophobic state, and the micro-pillars were hydrophilic or hydrophobic. Adding nanostructures on the microstructures can significantly increase the static CA, and a hydrophilic material can be converted to a superhydrophobic one.

Table 2 Static contact-angle results of the micro-pillars and nano-cylinders on micro-pillars

Structure	Sample	$h1$, μm	a, μm	b, μm	d, nm	$h2$, nm	L, nm	CA, °
nano-cylinders on micro-pillars	1	20	20	10	400	1500	500	150.2
	2	20	20	20	400	1500	500	151.7
	3	40	20	10	400	1500	500	152.6
	4	40	20	20	400	1500	500	152.3
micro-pillars	5	20	20	10	—	—	—	72.3
	6	20	20	20	—	—	—	63.1
	7	40	20	10	—	—	—	125.6
	8	40	20	20	—	—	—	136.7

Note: — means that samples 5–8 do not have nanostructures.

doi: 10.1049/mnl.2020.0345

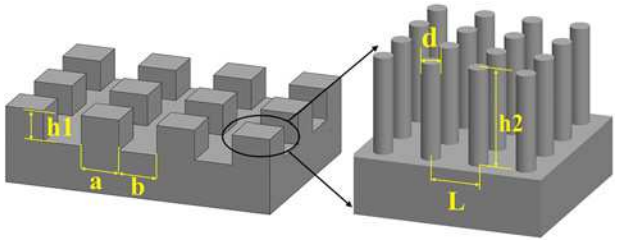

Fig. 10 *Definitions of the quantities of samples 1–8*

The size of structures also affected the hydrophilic and hydrophobic properties. The wettability of a pure microstructure surface was greatly affected by the height of micro-pillars. Small micro-pillars give a hydrophilic structure, whereas tall micro-pillars give a hydrophobic structure having a high CA. However, the wettability of high aspect ratio nano-cylinders on micro-pillars was unaffected by the micro-pillar height, and the structure remained superhydrophobic.

The effect of the structure size on wettability can be explained by the different wetting states of structures. Wetting analysis indicates that small microstructures allow water to surround the micro-pillar structure to produce a Wenzel state [27]. High aspect ratio nano-cylinders on micro-pillars demonstrate a hybrid state at which water sits on the nanoscale cylinders with partially immersed microscale pillars [28].

4. Conclusion: High aspect ratio nano-cylinders on a micro-pillar structure were prepared on a 4-inch silicon wafer through a PS colloidal crystal mask. An experimental device was designed for the stripping of PS nanospheres and liquid drainage to realise two key processes: the transfer of PS nanospheres from the silicon master to the liquid surface and the deposition of the PS colloidal crystal mask on the micro-pillars. The optimal drop rate of the liquid surface was determined through experiments to create a uniform PS colloidal crystal mask on the micro-pillars. Samples with controllable size were fabricated by adjusting key process parameters, such as RIE time and Ag-assisted etching time. Wetting-performance tests were performed to examine the wettability of the large area high aspect ratio nano-cylinders on micro-pillars. Results revealed that the structures obtained were superhydrophobic. Compared with micro-pillars, high aspect ratio nano-cylinders on micro-pillars can significantly enhance the hydrophobic performance of the material, and the height of the micro-pillars had little effect on wettability. The addition of nanostructures to microstructures caused the change from hydrophilic to superhydrophobic. The large-area high aspect ratio nano-cylinders on micro-pillars have potential applications in the fields of anti-icing and anti-fog.

5. Acknowledgments: We are grateful for the support from the National Natural Science Foundation of China (grant nos. 51875478 and 51735011), the Aeronautical Science Foundation of China (grant no. 2017ZC53036), the National Basic Research Project (JCKY2018**18), and the Fundamental Research Funds of Shenzhen City (JCYJ2016022917313).

6 References

[1] Zuo Z., Liao R., Guo C., *ET AL.*: 'Fabrication and anti-icing property of coral-like superhydrophobic aluminum surface', *Appl. Surf. Sci.*, 2015, **331**, pp. 132–139
[2] Shi W., Wang L., Guo Z, *ET AL.*: 'Excellent anti-icing abilities of optimal micropillar arrays with nanohairs', *Adv. Mater. Interfaces*, 2015, **2**, (18), pp. 1500352.1–8
[3] Sun J., Wang L., Hu K., *ET AL.*: 'Fabrication of superhydrophobic surfaces on copper substrates via flow plating technology', *Micro Nano Lett.*, 2015, **10**, (2), pp. 88–92
[4] Martin S., Bhushan B.: 'Fluid flow analysis of a shark-inspired microstructure', *J. Fluid Mech.*, 2014, **756**, pp. 5–29
[5] Zhang Y., Wei S., Liu F., *ET AL.*: 'Superhydrophobic nanoporous polymers as efficient adsorbents for organic compounds', *Nano Today*, 2009, **4**, (2), pp. 135–142
[6] Cui Y., Wei Q.Q., Park H.K., *ET AL.*: 'Nanowire nanosensors for highly sensitive and selective detection of biological and chemical species', *Science*, 2001, **293**, (5533), pp. 1289–1292
[7] Bhushan B., Jung Y.C., Koch K.: 'Micro-, nano- and hierarchical structures for superhydrophobicity, self-cleaning and low adhesion', *Philos. Trans. R. Soc. Lond. A, Math. Phys. Eng. Sci.*, 2009, **367**, (1894), pp. 1631–1672
[8] Zhang F., Jiang Y., Liu X., *ET AL.*: 'Hierarchical nanowire arrays as three-dimensional fractal nanobiointerfaces for high efficient capture of cancer cells', *Nano Lett.*, 2016, **16**, (1), pp. 766–772
[9] Li J., Wang W., Mei X., *ET AL.*: 'Artificial compound eyes prepared by a combination of air-assisted deformation, modified laser swelling, and controlled crystal growth', *ACS Nano*, 2019, **13**, (1), pp. 114–124
[10] Yoshino M., Aravindan S.: 'Nanosurface fabrication of hard brittle materials by structured tool imprinting', *Trans. ASME, J. Manuf. Sci. Eng.*, 2004, **126**, (4), pp. 760–765
[11] Wan Y., Xu L., Yu H.: 'Fabrication of superhydrophobic aluminium alloy surface by twice nanosecond laser scanning', *Micro Nano Lett.*, 2018, **13**, (4), pp. 469–472
[12] Patil D., Aravindan S., Wasson M.K., *ET AL.*: 'Fast fabrication of superhydrophobic titanium alloy as antibacterial surface using nanosecond laser texturing', *J. Micro Nano-Manuf.*, 2018, **6**, (1), pp. 011002.1–8
[13] Patil D., Sharma A., Aravindan S., *ET AL.*: 'Development of hot embossing setup and fabrication of ordered nanostructures on large area of polymer surface for antibiofouling application', *Micro Nano Lett.*, 2019, **14**, (2), pp. 191–195
[14] Ahn S.W., Lee K.D., Kim J.S., *ET AL.*: 'Fabrication of subwavelength aluminum wire grating using nanoimprint lithography and reactive ion etching', *Microelectron. Eng.*, 2005, **78-79**, pp. 314–318
[15] Zhang R., Chu J., Wang Z., *ET AL.*: 'Simple process for single-layer nanowire gratings', *Micro Nano Lett.*, 2015, **10**, (5), pp. 272–275
[16] Wu W., Dey D., Memis O.G., *ET AL.*: 'Fabrication of large area periodic nanostructures using nanosphere photolithography', *Nanoscale Res. Lett.*, 2008, **3**, (10), pp. 351–354
[17] Wang F., Jiang S., Han J., *ET AL.*: 'Facile and low-cost fabrication of uniform silicon micro/nanostructures by nanopitting-assisted wet chemical etching', *Micro Nano Lett.*, 2018, **13**, (9), pp. 1296–1301
[18] Feng L., Li S.H., Li Y.S., *ET AL.*: 'Super-hydrophobic surfaces: from natural to artificial', *Adv. Mater.*, 2002, **14**, (24), pp. 1857–1860
[19] Chen Z., Cao M.: 'Synthesis, characterization, and hydrophobic properties of Bi2S3 hierarchical nanostructures', *Mater. Res. Bull.*, 2011, **46**, (4), pp. 555–562
[20] Sun M.H., Luo C.X., Xu L.P., *ET AL.*: 'Artificial lotus leaf by nanocasting', *Langmuir*, 2005, **21**, (19), pp. 8978–8981
[21] Cho H., Kim D., Lee C., *ET AL.*: 'A simple fabrication method for mechanically robust superhydrophobic surface by hierarchical aluminum hydroxide structures', *Curr. Appl. Phys.*, 2013, **13**, (4), pp. 762–767
[22] Song J.L., Xu W.J., Lu Y.: 'One-step electrochemical machining of superhydrophobic surfaces on aluminum substrates', *J. Mater. Sci.*, 2012, **47**, (1), pp. 162–168
[23] He Y., Jiang C., Yin H., *ET AL.*: 'Superhydrophobic silicon surfaces with micro–nano hierarchical structures via deep reactive ion etching and galvanic etching', *J. Colloid Interface Sci.*, 2011, **364**, (1), pp. 219–229
[24] Wu P.H., Cheng C.W., Chang C.P., *ET AL.*: 'Fabrication of large-area hydrophobic surfaces with femtosecond-laser-structured molds', *J. Micromech. Microeng.*, 2011, **21**, (11), pp. 115032.1–7
[25] He Y., Zhu B., Zeng X., *ET AL.*: 'Fabrication of large-area, close-packed, monolayer colloidal crystals via a hybrid method of spin coating and peeling-draining', *Thin Solid Films*, 2017, **639**, pp. 98–106
[26] Huang Z., Fang H., Zhu J.: 'Fabrication of silicon nanowire arrays with controlled diameter, length, and density', *Adv. Mater.*, 2007, **19**, (5), pp. 744–748
[27] He Y., Jiang C., Wang S., *ET AL.*: 'Control wetting state transition by micro-rod geometry', *Appl. Surf. Sci.*, 2013, **285**, pp. 682–687
[28] He Y., Jiang C., Yin H., *ET AL.*: 'Superhydrophobic silicon surfaces with micro–nano hierarchical structures via deep reactive ion etching and galvanic etching', *J. Colloid Interface Sci.*, 2011, **364**, (1), pp. 219–229